Radio Science, Volume 33, Number 3, Pages 745–751, May–June 1998

Global maps of microwave land surface emissivities: Potential for land surface characterization

Catherine Prigent [1]
NASA Goddard Institute for Space Studies, Columbia University, New York

William B. Rossow
NASA Goddard Institute for Space Studies, New York

Elaine Matthews
Center for Climate System Research, NASA Goddard Institute for Space Studies
Columbia University, New York

Abstract. Microwave land surface emissivities are derived from special sensor microwave imager (SSM/I) observations. Cloud-free SSM/I observations are first isolated with the help of collocated visible/infrared satellite observations (International Satellite Cloud Climatology Project (ISCCP) data). Then, the cloud-free atmospheric contribution is calculated from an estimate of the local atmospheric temperature-humidity profile (National Centers for Environmental Prediction (NCEP) analyses). Finally, with the surface skin temperature derived from IR observations (ISCCP estimate), the surface emissivity is calculated for all the SSM/I channels. The method is applied to the SSM/I data for the globe for October 1991. Correspondences between geographical patterns of the emissivities and surface characteristics are briefly analyzed to investigate the potential of microwave emissivities to monitor vegetation phenology and surface properties at regional and continental scales.

1. Introduction

Estimating land surface emissivities from satellite microwave measurements is of major interest for two main reasons. First, the ability to retrieve atmospheric parameters (water vapor, cloud liquid water, precipitation) above land depends in large part on the capability to estimate surface emissivity. If the surface emissivities can be determined accurately enough, cloud liquid water and precipitation retrieval might be extended to land areas. Second, land surface emissivities derived from microwave satellite measurements could be used to monitor variations of surface and vegetation properties at regional and continental scales. Most satellite studies carried out over land have focused on the use of simple indices derived from linear combinations of microwave satellite measurements (the microwave vegetation index (MVI) for instance) [*Choudhury and Tucker*, 1987; *Choudhury*, 1989]. However, atmospheric effects (especially cloud cover) and surface temperature may contribute substantially to the variations of these indices, casting doubt on their interpretation solely in terms of surface properties [e.g., *Kerr and Njoku*, 1993].

A method is proposed to directly estimate the microwave emissivities from special sensor microwave imager (SSM/I) observations by removing the contributions from the atmosphere, clouds, and rain us-

[1] On leave from Departement de Radioastronomie Millimetrique, Centre National de la Recherche Scientifique, Observatoire de Paris, Paris, France.

Paper number 97RS02460.
0048-6604/98/97RS-02460$11.00

ing ancillary observations. The method has been described in details by *Prigent et al.* [1997], where results have been limited to Africa and part of Europe. In the present study, the method is outlined, and global results are presented for October 1991. The International Satellite Cloud Climatology Project (ISCCP) data are used to detect the presence of clouds and to determine the surface skin temperature. The National Center for Numerical Prediction (NCEP) analyses provide the atmospheric profiles of temperature and water vapor to estimate the gaseous atmospheric contribution. Correspondences between microwave emissivities and surface characteristics are briefly analyzed to explore the potential of microwave observations for monitoring vegetation phenology, wetlands, snow, and sea ice.

2. Principles and Data

Over a flat surface, the radiative transfer for a nonscattering plane-parallel atmosphere can be expressed in terms of brightness temperature for each orthogonal polarization P (P stands for either horizontal, H, or vertical, V):

$$Tb_P = Tsurf \times emis_P \times e^{-\tau(0,H)/\mu}$$

$$+Tatm\_down \times (1 - emis_P) \times e^{-\tau(0,H)/\mu} + Tatm\_up \quad (1)$$

where $Tatm\_down = \int_0^H T(z)\alpha(z)e^{-\tau(0,z)/\mu}dz$ and $Tatm\_up = \int_0^H T(z)\alpha(z)e^{-\tau(z,H)/\mu}dz$. Tb_P is the brightness temperature measured by the satellite for polarization P; $Tsurf$ is the surface "skin" temperature; $emis_P$ is the surface emissivity for polarization P; $\mu = \cos(\theta)$; θ being the incident angle on the surface; $\alpha(z)$ is the atmospheric absorption by gases and nonprecipitating particles at altitude z; $T(z)$ is the atmospheric temperature at altitude z; and $\tau(z_0, z_1) = \int_{z_0}^{z_1} \alpha(z)dz$ is the atmospheric opacity from z_0 to z_1. This equation leads to

$$emis_P = \frac{Tb_P - Tatm\_up - Tatm\_down \times e^{-\tau(0,H)/\mu}}{e^{-\tau(0,H)/\mu} \times (Tsurf - Tatm\_down)} \quad (2)$$

The method consists of solving (2) for the surface emissivity for each SSM/I channel using ancillary data to specify the atmospheric and surface parameters.

The Defense Meteorological Satellite Program satellites (DMSP) observe the Earth twice daily from near-polar orbits. The SSM/I instruments on board these satellites sense the atmospheric and surface emissions at 19.35, 22.235, 37.0, and 85.5 GHz with both horizontal and vertical polarizations, with the exception of 22 GHz, which is at vertical polarization only [*Hollinger et al.*, 1987]. The observing incident angle on the Earth is close to 53°, and the elliptical fields of view decrease in size proportionally with frequency, from 43×69 to 13×15 km.

In the ISCCP data, cloud parameters and related quantities are retrieved from visible (VIS) (~0.6μm wavelength) and infrared (IR) (~11μm wavelength) radiances provided by the set of polar and geostationary meteorological satellites [*Rossow and Schiffer*, 1991]. The ISCCP data set is used not only to discriminate clear and cloudy scenes but also to estimate surface skin temperature. The pixel level data set (the DX data set) is used for its resolution of about 30 km and its sampling interval of 3 hours. The DX ISCCP data sets are available for each geostationary satellite (up to five satellites in orbit at a time) and for the two NOAA polar orbiting satellites. A detailed description of the ISCCP data is provided by *Rossow et al.* [1996].

The atmospheric profiles used in this study are extracted from the NCEP reanalysis data set [*Kalnay et al.*, 1996]. It includes surface pressure, temperatures, and relative humidities for eight levels up to 300 mbar (middle and lower troposphere), every 6 hours, at a spatial resolution of 2.5° latitude and longitude. In our previous study [*Prigent et al.*, 1997], the atmospheric profiles were extracted from the TIROS operational vertical sounder (TOVS) system as gridded by ISCCP [*Rossow et al.*, 1996]. However, unrealistically high standard deviations in the TOVS water vapor abundances were noticed over desert areas, which were affecting the retrieval of surface emissivities, especially at 85 GHz. The NCEP reanalyses do not show similar behavior.

To compare products at the same location over a month, the map projection of the ISCCP DX products is used [*Rossow et al.*, 1996], corresponding to a spacing of 25-30 km. This grid spacing is fully compatible with the SSM/I observations which are sampled at 25 km. For a month, the following procedure is applied to each DX ISCCP data set (corresponding to each geostationary satellite and the two NOAA polar orbiters). For each SSM/I pixel (day and night), the corresponding ISCCP DX pixels are selected for the time closest to the SSM/I overpass

time. Then SSM/I pixels are selected that correspond to ISCCP pixels that are clear or have only high clouds (cloud top temperature $\leq$260 K) with an optical thickness less than one. High and thin ice clouds (i.e., thin cirrus) can be tolerated because of their negligible effect at SSM/I frequencies. At the time of SSM/I overpass at low and middle latitudes (close to sunrise and sunset up to middle latitude), rapid changes of the surface temperature can be observed within the 3-hour gap between two consecutive DX images (up to 30 K over the north African desert). Selecting the closest-in-time geostationary image to derive the surface temperature can produce large errors in the emissivity retrieval. Therefore, because of the availability of the DX data every 3 hours from the geostationary satellites, a linear interpolation between the two ISCCP surface temperature estimations to the precise time of the SSM/I overpass is calculated. Using the closest NCEP profile (in time and space) and the MPM 93 model [*Liebe et al.*, 1993] for gaseous absorptions, the cloud-free atmospheric contribution is calculated for each SSM/I frequency. Equation (2) is then solved for the emissivity for each SSM/I frequency and polarization. For each 30x30 km cell, the average and standard deviation of the emissivity is calculated for the month for each channel and for each DX data set. Finally, the results corresponding to each DX data set are merged: For each geographical location and for each SSM/I channel, a weighted mean of the available surface emissivities is calculated.

3. Results and Discussion

Maps of the polarization differences (vertical minus horizontal polarization) of the retrieved emissivities at 19 GHz and 85 GHz are presented for October 1991 (Plates 1a and 1b) for measurements from the F10 DMSP satellite. The vegetation classification map [*Matthews*, 1983] is also displayed (Plate 1c). The vegetation data set distinguishes 30 classes which are grouped into 10 classes for this study, as indicated in Table 1. The microwave emissivities are retrieved not only above the continents but also above the ocean when sea ice is present (the ice cover information from the NOAA operational analysis is used, as reported in the ISCCP data set). The large hole in the microwave surface emissivity maps in the northern hemisphere around 70°E corresponds to the absence of geostationary satellite data in this area. Only the two NOAA polar orbiters are available in this region: Although the overpass times of the NOAA morning orbiter and the DMSP satellite are within 2 hours over the equator, when the NOAA morning polar orbiter is in its ascending mode (moving northward), the DMSP satellite is in its descending mode. Thus the number of coincident overpasses at middle latitudes is very small. Processing the two DMSP satellites that are in orbit (the F10 and the F11 for that period) should reduce this problem.

The mode value of the standard deviation of the retrieved emissivities for October 1991 is 0.008 at 19 and 37 GHz and 0.017 at 22 and 85 GHz, whatever the polarization. The more sensitive the channel to the atmosphere, the larger the standard deviation over a month, suggesting some residual errors associated with the atmosphere. A sensitivity analysis of the retrieved emissivities to the various input parameters (the SSM/I instrumental errors, the surface temperature, the water vapor profile, and the water vapor absorption model) has been conducted, and the results are discussed by *Prigent et al.* [1997].

The following comparisons focus on the correspondences between the geographical patterns of the emissivity and variations in surface characteristics. Because of the lack of direct information about surface emissivity at these spatial scales, our comparisons can only be indirect attempts to verify the retrieved products by showing that the emissivity patterns can be explained by recognized changes in surface characteristics.

Regions of bare soil (northern Africa, the Arabian Peninsula, the Australian desert) show high polarization differences (Plates 1a and 1b) associated with low emissivities in the horizontal polarization (not shown) when compared with vegetated areas. Although rather stable in time, deserts show significant spatial variations (for instance, compare the Australian desert and the Sahara). These differences must be further investigated in terms of soil and rock materials. On the other hand, densely vegetated zones (the tropical rain forest) exhibit low polarization differences: The vegetation elements are randomly oriented within the vegetation canopy and emit almost independently from polarization, and at the same time attenuate the polarized emission from the underlying soil. Histograms of the 19 and 85 GHz emissivities are presented in Figure 1 for the 10 surface types (Table 1). With decreasing biomass density (from class 1 to class 9) the horizontal polar-

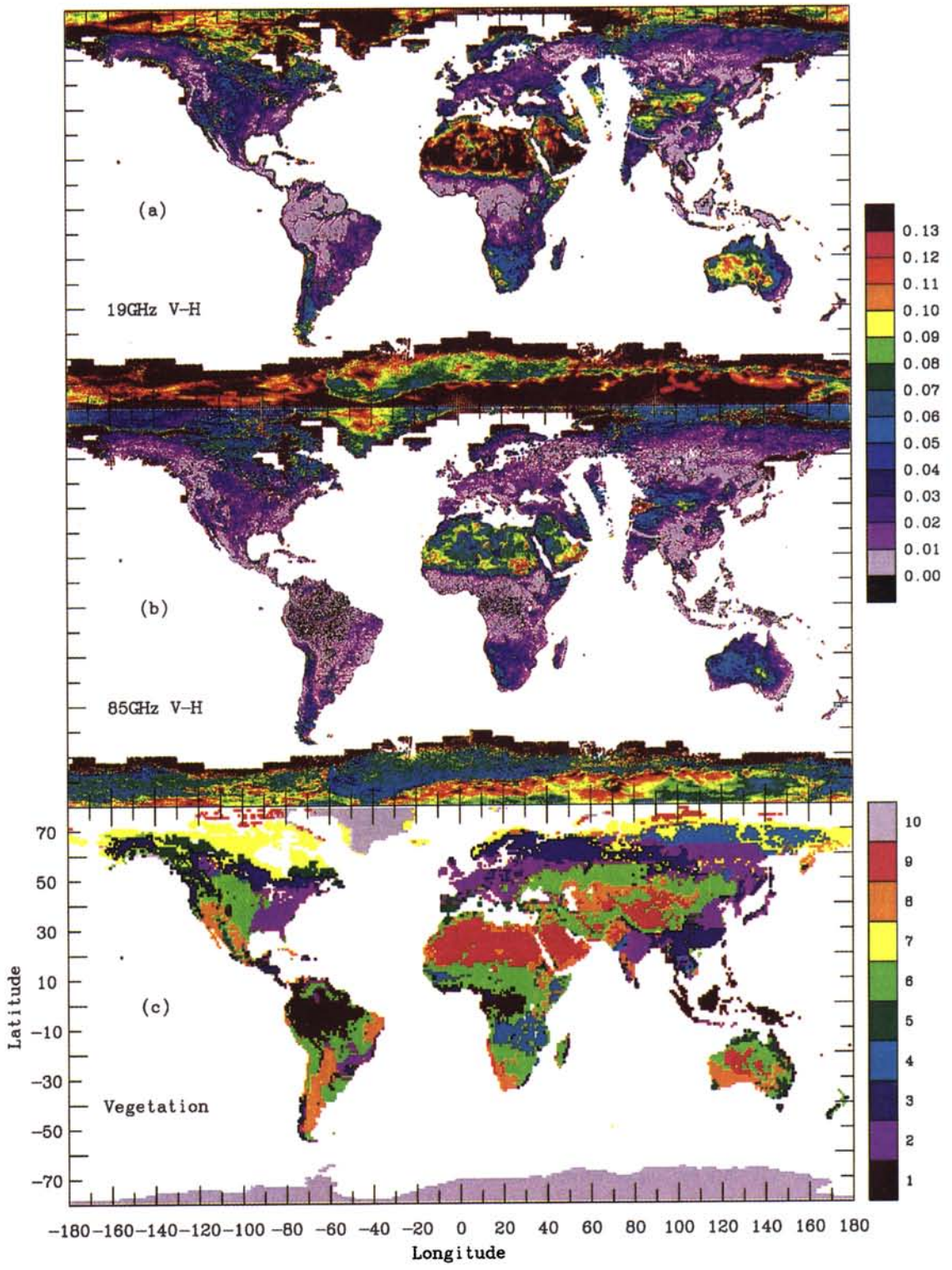

Plate 1. Polarization differences of the emissivities (vertical minus horizontal polarization) at (a) 19 GHz and (b) 85 GHz, for October 1991. (c) Vegetation map for the ten classes defined in Table 1.

Table 1. The 10 Types of Surfaces

Surface Type	Description
1	tropical/subtropical evergreen broad-leaved forest
2	deciduous forest
3	evergreen broad-leaved and needle-leaved forest
4	deciduous woodland
5	sclerophyllous woodland and forest
6	wooded and nonwooded grassland
7	tundra and mossy bog
8	boreal and xeromorphic shrubland
9	nonvegetated desert
10	ice

Derived from *Matthews* [1983]

ization decreases, the vertical polarization increases, and the polarization difference increases. Most histograms are well defined with only one mode. The widths of the histograms are much larger than are the standard deviations of the emissivities over the month at individual locations: Dispersion in the histograms thus represents actual surface variability. Although covering a large area, the sparse vegetation type (class 8) does not exhibit narrow distributions: Vegetation in these arid zones is not well defined and can encompass a very broad range of conditions [cf. *Matthews and Rossow*, 1987]. The tundra regions (class 7) also show broad histograms that are related to the presence of snow and ice cover. The grassland (class 6) histogram of horizontal polarization has a rather long tail corresponding to relatively low emissivities. Comparison of Plates 1a, 1b and 1c shows that the desert-like emissivity signature in northern Africa and Australia are more extensive than the corresponding desert areas in the vegetation map. While the sensitivity of the microwave emissivities to very sparse, arid vegetation is expected to be low, the vegetation classification may also have to be reexamined, particularly with respect to geographic transitions and recent changes.

Various roughness scales are involved within a single field of view, from the small-scale roughness related to surface irregularities small compared with the wavelength to the large-scale topographic effect.

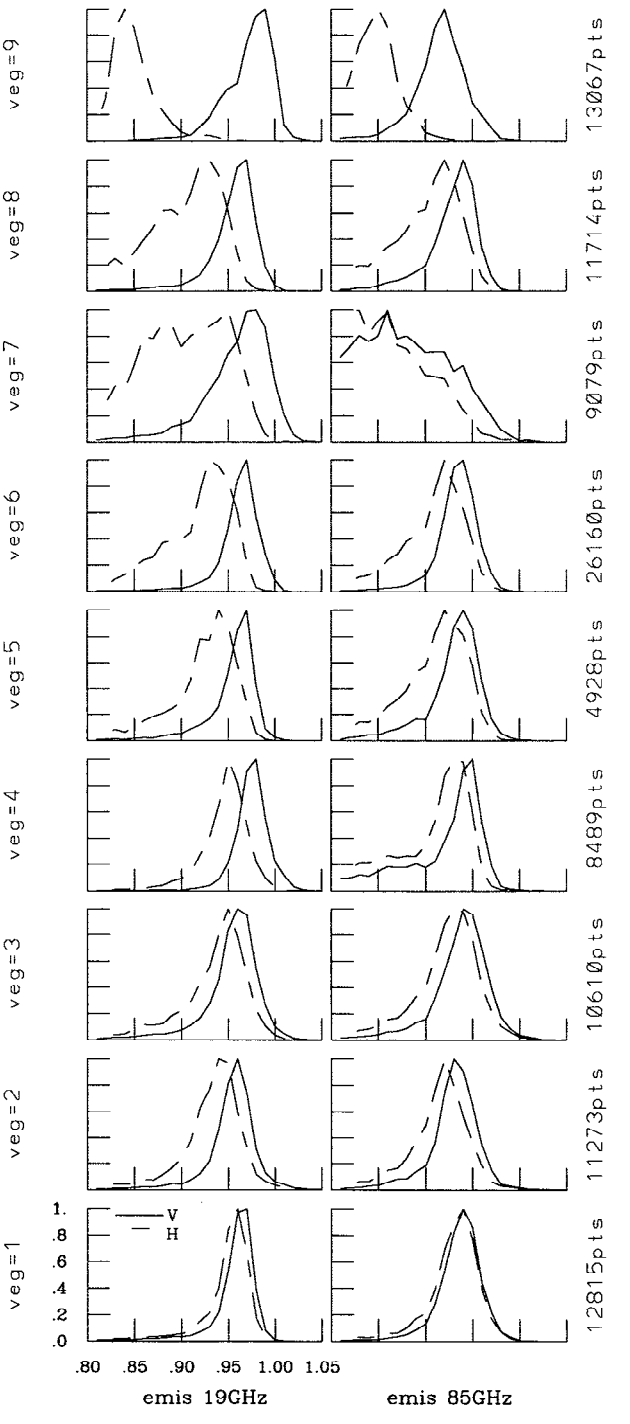

Figure 1. Normalized histograms of the retrieved emissivities at 19 and 85 GHz for both polarizations for the 10 surface types (October 1991). The number of pixels in each class is added.

Large-scale topographic roughness reduces the difference between polarizations. In vegetated areas this emissivity feature is difficult to identify because the vegetation usually changes with elevation and because the emissivity difference in polarizations is already reduced by the vegetation. For sparsely vegetated or nonvegetated areas, however, this effect can be observed as decreasing polarization differences with increasing topographic roughness. For example, the Sahara is associated with high polarization differences, but these differences decrease over the Tibesti and the Ahaggar mountain areas.

Microwave observations have been shown to be valuable for delineating flooded areas [see, for examples, *Choudhury*, 1989]. At microwave frequency, open water and flooding decrease the emissivities in both polarizations and increase the polarization differences, especially at lower frequencies. This response is due to differences in the dielectric properties of water as compared with soil and vegetation and to the flatness of standing water surfaces. On the 19 GHz emissivity maps (Plate 1a), the main hydrological features are well delineated: For instance, the Congo River and the Amazon appear very clearly.

Although several snow and ice studies have been based on microwave satellite observations [*Cavalieri et al.*, 1984; *Comiso*, 1986; *Grody and Basist*, 1996], the microwave signature of these surface types is still not fully understood. In our emissivity results, the ice- and snow-covered areas show a wide spatial and temporal diversity of signatures. The snow-covered land and the sea ice areas are characterized by large variations of the surface emissivity over the month (not shown here), even in areas where the NOAA ice/snow reports indicate full coverage of snow or ice throughout the month. In contrast, ice-covered lands (Antarctica and Greenland) exhibit much more stable temporal behavior, although spatially variable. Compared with sea ice, land ice at this period of the year has a generally lower emissivity in both polarizations and for each frequency, along with larger polarization differences. These characteristics must be explored in more detail on an annual basis to investigate the potential of these emissivity retrievals to estimate the ice and snow properties.

4. Conclusions and Possibilities

Microwave emissivities of the land surface are estimated from SSM/I observations by removing contributions from the atmosphere, clouds, and rain using ancillary data from ISCCP and NCEP. Global maps of the microwave emissivities are presented for October 1991. Correspondences between geographical patterns of the microwave emissivities with variations in surface characteristics are briefly analyzed. In the absence of direct measurements of surface emissivities at these larger spatial scales, these comparisons help verify the quality of the retrieved products. The monthly standard deviations of the emissivities have a mode value ≤ 0.017 for all the channels. We plan to apply this method to produce global emissivity maps for every month over several years. The intra-annual and interannual variabilities of the emissivities will be investigated. The feasibility of estimating microwave emissivities over land offers a number of interesting possibilities from monitoring the land surface itself, in addition to their use in atmospheric and cloud parameter retrievals.

Correspondences between the microwave emissivities and vegetation distributions suggest the possibility of using microwave emissivities to monitor vegetation phenology at regional and continental scale. The SSM/I land emissivities have also shown a strong sensitivity to flooding and to snow cover and sea ice characteristics and could be further used to monitor these parameters.

With accurate estimates of land microwave emissivities (and surface skin temperature), it is possible to consider extending atmospheric and cloud property retrievals from microwave measurements developed over ocean to land areas. The ability to estimate atmospheric parameters essentially depends on the contrast between the radiance of the atmosphere and the radiance of the surface. As a result, the accuracy of atmospheric parameter retrieval will depend strongly on atmospheric and surface conditions. A variational inversion method is now under development to retrieve water vapor and cloud liquid water from the SSM/I observations over land.

Acknowledgment. We are grateful to A. Walker for her help in processing the ISCCP data sets.

References

Cavalieri, D. J., P. Gloersen and W. J. Campbell, Determination of sea ice parameters with the Nimbus-7 SMMR, *J. Geophys. Res.*, 89, 5355-5369, 1984.

Choudhury, B. J., Monitoring global land surface using Nimbus-7 37 GHz data: Theory and examples, *Int. J. Remote Sens.*, 10, 1579-1605, 1989.

Choudhury, B. J. and C. J. Tucker, Monitoring global vegetation using Nimbus-7 37 GHz data: Some empirical relations, *Int. J. Remote Sens.*, 8, 1085-1090, 1987.

Comiso, J. C., Characteristics of Arctic winter sea ice from satellite multispectral microwave observations, *J. Geophys. Res.*, 91, 975-994, 1986.

Grody, N. C. and A. N. Basist, Global identification of snow cover using SSM/I measurements, *IEEE Trans. Geosci. Remote Sens.*, 34, 237-249, 1996.

Hollinger, J. P., R. Lo, G. Poe, R. Savage and J. Pierce, *Special Sensor Microwave/Imager User's Guide*, Nav. Res. Lab., Washington, D. C., 1987.

Kalnay, E. et al., The NCEP/NCAR 40-year reanalysis project, *Bull. Am. Meteorol. Soc.*, 77, 437-470, 1996.

Kerr, Y. H. and E. G. Njoku, On the use of passive microwave at 37 GHz in remote sensing of vegetation, *Int. J. Remote Sens.*, 14, 1931-1943, 1993.

Liebe, H. J., G. A. Hufford and M. G. Cotton, Propagation modeling of moist air and suspended water/ice particles at frequencies below 1000 GHz, paper presented at the Specialist Meeting of the Electromagnetic Wave Propagation Panel, Adv. Group for Aerosp. Res. and Dev., Palma de Mallorca, Spain, 1993.

Matthews, E., Global vegetation and land use: New high-resolution data bases for climate studies, *J. Clim. Appl. Meteorol.*, 22, 474-486, 1983.

Matthews, E. and W. B. Rossow, Regional and seasonal variations of surface reflectance from satellite observations at 0.6 microns, *J. Clim. Appl. Meteorol.*, 26, 170-202, 1987.

Prigent, C., W. B. Rossow and E. Matthews, Microwave land surface emissivities estimated from SSM/I observations, *J. Geophys. Res.*, 102, 21 867-21 890, 1997.

Rossow, W. B. and R. A. Schiffer, ISCCP cloud data products, *Bull. Am. Meteorol. Soc.*, 72, 2-20, 1991.

Rossow, W. B., A. W. Walker, D. E. Beuschel and M. D. Roiter, International Satellite Cloud Climatology Project (ISCCP). Document on new cloud datasets, NASA Goddard Inst. for Space Stud., New York, 1996.

E. Matthews, Center for Climate System Research, NASA Goddard Institute for Space Studies, Columbia University, New York, N.Y., 10025. (email: ematthews@giss.nasa.gov)

C. Prigent, NASA Goddard Institute for Space Studies, Columbia University, New York, N.Y., 10025. (email: cprigent@giss.nasa.gov)

W. B. Rossow, NASA Goddard Institute for Space Studies, New York, N.Y., 10025. (email: wrossow@giss.nasa.gov)

(Received March 7, 1997; revised July 21, 1997; accepted September 4, 1997.)